Pattern Recognition Letters 29 (2008) 1659–1666

Contents lists available at ScienceDirect

Pattern Recognition Letters

journal homepage: www.elsevier.com/locate/patrec

Anisotropic virtual electric field for active contours

Guopu Zhu [a], Shuqun Zhang [b,*], Qingshuang Zeng [c], Changhong Wang [c]

[a] GuangDong Key Laboratory of Information Security Technology, Sun Yat-Sen University, Guangzhou 510006, China
[b] Department of Computer Science, College of Staten Island, City University of New York, Staten Island, NY 10314, USA
[c] Space Control and Inertial Technology Research Center, Harbin Institute of Technology, Harbin 150001, China

ARTICLE INFO

Article history:
Received 15 December 2006
Received in revised form 17 January 2008
Available online 30 April 2008

Communicated by H.H.S. Ip

PACS:
40.000

Keywords:
Active contours
Virtual electric field
Gradient vector flow
Image segmentation

ABSTRACT

A novel external force called anisotropic virtual electric field (AVEF) is proposed for active contours by incorporating the geometric information of the image edge map into a virtual electric field (VEF) model. The proposed AVEF model has the advantage of preventing active contours from moving across object boundary's weak edges with strong neighbors while keeping the desirable properties of the VEF model, such as large capture range and fast computation time. The experiments conducted on synthetic and real images show the high performance of the AVEF model on image segmentation.

© 2008 Elsevier B.V. All rights reserved.

1. Introduction

Active contours, or snakes, have been widely researched and applied in image processing and computer vision since they were first introduced by Kass et al. (1988). The applications of active contours include image segmentation (Xu and Prince, 1998b; Chan and Vese, 2001), shape modeling (Malladi et al., 1995), visual tracking (Paragios and Deriche, 2000; Mansouri, 2002) and motion estimation (Mansouri et al., 2003; Cremers and Soatto, 2005). An active contour is a dynamic curve driven by mathematically-formulated forces to conform to an object boundary. The driving forces are generally derived from minimizing an energy functional with respect to the dynamic curve. In active contour models that are closely based on the work of Kass, the driving forces are usually defined as the negative gradient of the energy functional. A variety of other driving forces (Xu and Prince, 1998b; Park and Chung, 2002) have been also proposed to improve the performance of the Kass snakes.

This paper mainly addresses the issue of designing new driving force for active contour models. In image segmentation, active contours are forced to evolve from a given initial position to the desired object boundary by "internal forces" defined to smooth the dynamic curve and by "external forces" defined to make the dynamic curve approach the desired object boundary. The key forces of active contours are the external forces, which have flexibility in design and decisive influence on segmentation performance. Many external forces for active contours have been designed, among which the gradient vector flow (GVF) (Xu and Prince, 1998b) and virtual electric field (VEF) (Park and Chung, 2002) are in particular closely related to this paper. The GVF is computed as a diffusion of the gradient vectors of a gray-level or binary edge map derived from the image. With respect to the Kass active contour, the GVF has been shown to have better capture range and better "convergence to concavity" (that is, convergence to object boundaries which have concave regions). Many modifications of the GVF have been proposed (Xu and Prince, 1998a; Xie and Mirmehdi, 2004; Chuang and Lie, 2004; Ray and Acton, 2004; Li et al., 2005; Tang et al., 2006; Cheng and Foo, 2006). For example, the motion GVF (Ray and Acton, 2004) embeds motion information into the GVF model so that it can deal with the tracking problem more effectively. On the other hand, the VEF, which was almost simultaneously introduced by several researchers (Park and Chung, 2002; Yuan and Lu, 2002; Honea et al., 2002), defines an external force by simulating the electric field in physics. Several improvements (Zhu et al., 2006a; Chang and Valentino, 2006) to the VEF model have been also proposed. Recently, the VEF active contour was applied to image segmentation in particle systems (Jalba et al., 2004). Although the GVF and the VEF are designed according to different principles, they have some similar properties. For example, they have similar performance (extended capture range and capability of converging to concavity) in application, and

* Corresponding author. Tel.: +1 718 982 3178; fax: +1 718 982 2856.
E-mail address: zhangs@mail.csi.cuny.edu (S. Zhang).

0167-8655/$ - see front matter © 2008 Elsevier B.V. All rights reserved.
doi:10.1016/j.patrec.2008.04.009

neither can be written as the negative gradient of an energy function with respect to the boundary of the contour. However, it has been observed that the GVF requires more processing time than the VEF due to its requirement of optimizing the diffusion equation (Park and Chung, 2002).

Recently some modified GVF models have addressed the problem of boundary leakage near weak edges with strong neighbors (Xie and Mirmehdi, 2004; Li et al., 2005). Some improved results have been obtained by the region-aided GVF (Xie and Mirmehdi, 2004), in which a robust region-based segmentation method was used. However, none of the VEF-based external forces have been able to solve the boundary leakage problem. This paper attempts to address this problem by proposing a novel external force called anisotropic virtual electric field (AVEF), which is developed from the original VEF. In general terms, our approach begins by extracting salient curves from the pixels with high intensities in the image edge map. We then extract the geometric information of these curves and incorporate it into the VEF model to generate the AVEF. The extracted geometric information of the edge map is employed to influence the field forces to point perpendicularly to the image edges when the field forces are near the edges (even near weak edges with strong neighbors). It will be shown that the proposed AVEF has the advantage of preventing the active contour from moving across the object boundary's weak edges with strong neighbors, and has improved performance relative to the original VEF. We note that geometric information has been also recently shown to improve the performance of the Kass and GVF models (Tang et al., 2006; Cheng and Foo, 2006; Jacob et al., 2004; Park et al., 2001). We implement the proposed AVEF on the Kass parametric active contour model (Kass et al., 1988). It can be easily modified for implementation on the level-set-based geometric active contours (Caselles et al., 1993, 1997; Paragios and Deriche, 2002; Zhu et al., 2006b) as in the paper (Paragios et al., 2004).

The paper is organized as follows: In Section 2, we briefly describe some background of the Kass active contour and the VEF. In Section 3, we introduce the proposed AVEF external force. The experimental results conducted on synthetic and real images are presented in Section 4. We provide conclusions in Section 5.

2. Background

2.1. Traditional active contours

Given a gray-value image I, a Kass active contour (Kass et al., 1988) is a closed dynamic curve $\boldsymbol{x} = [x(s), y(s)]$, $s \in [0, 1]$, which is defined to minimize the following energy functional:

$$E_{\mathrm{AC}}(\boldsymbol{x}) = \int_0^1 \frac{1}{2}[\alpha|\boldsymbol{x}'(s)|^2 + \beta|\boldsymbol{x}''(s)|^2] + E_{\mathrm{ext}}(\boldsymbol{x}(s))\mathrm{d}s, \tag{1}$$

where the first term in the integrand is the internal energy defined to keep the closed cure smooth, in which α and β are weighting parameters, and $\boldsymbol{x}'(s)$ and $\boldsymbol{x}''(s)$ are, respectively, the first and second derivatives of $\boldsymbol{x}$ with respect to s. The second term is the external energy defined to drive the dynamic curve to the desired image features. The typical external energy for a gray-value image is defined as

$$E_{\mathrm{ext}}(x, y) = -|\nabla[G_\sigma(x, y) * I(x, y)]|^2, \tag{2}$$

where $G_\sigma(x, y)$ is a two-dimensional Gaussian function with standard deviation σ, and ∇ is the gradient operator.

The energy functional E_{AC} can be minimized by evolving the dynamic curve $\boldsymbol{x}$ according a gradient descent method, which is written as

$$\boldsymbol{x}_t = \alpha\boldsymbol{x}'' - \beta\boldsymbol{x}'''' - \nabla E_{\mathrm{ext}}, \tag{3}$$

where $\boldsymbol{x}_t$ denotes the partial derivative of $\boldsymbol{x}$ with respect to the artificial time t, and the term $(\alpha\boldsymbol{x}'' - \beta\boldsymbol{x}'''')$ and $-\nabla E_{\mathrm{ext}}$ are called internal force and external force, respectively.

2.2. Virtual electric field

The Kass active contour has the problems of small capture range and poor convergence to concavity. In order to overcome these problems, Park and Chung (2002) replaced the external force $-\nabla E_{\mathrm{ext}}$ in Eq. (3) by the VEF, which treats each pixel in the edge map as an electric charge. For convenience, we will interchangeably use the terms pixel in the edge map and electric charge. Given an edge map $f(x, y)$, which is commonly defined as $|\nabla[G_\sigma(x, y) * I(x, y)]|^2$, in the image domain $R_i = (x, y)$, $(i = 1, \ldots, N)$. The virtual electric potential (VEP) of the edge map at location r is given by

$$P_{\mathrm{VEF}}(r) = \sum_{k:R_k \neq r}^{N} \frac{e_k}{4\pi\varepsilon_0} \frac{1}{|r - R_k|}, \tag{4}$$

where ε_0 is a positive constant that can be ignored here, and e_k is called electric charge, defined as the intensity of the edge map, i.e. $e_k = f(R_k)$. Computing the gradient of Eq. (4), we can obtain the corresponding VEF by

$$F_{\mathrm{VEF}}(r) = -\nabla P_{\mathrm{VEF}}(r) = \sum_{k:R_k \neq r}^{N} \frac{e_k}{4\pi\varepsilon_0} \frac{r - R_k}{|r - R_k|^3}. \tag{5}$$

Note that unlike the Kass external force $-\nabla E_{\mathrm{ext}}$ in Eq. (3), the VEF is not derived from minimizing an energy functional with respect to the boundary of the active contour. However, the VEF has been shown to exhibit better performance than the Kass external force, and similar performance to the GVF but with fast processing speed (Park and Chung, 2002).

3. Anisotropic virtual electric field

Although the VEF can significantly improve the performance of the Kass active contour, it still suffers from boundary leakage on weak edges with strong neighbors. As will be shown in the following experiments (Section 4), the VEF forces located at the weak edges are influenced to point to the strong neighboring edges, so that the VEF active contours are driven to move across the weak edge to its strong neighbors. It can be seen from Eqs. (4) to (5) that the VEF model so strictly conforms to the electric field model in physics that it disregards any geometric information from the edge map, which may reflect important relationships between adjacent electric charges. To exploit these relationships, we extract the geometric information of the edge map and then incorporate it into the original VEF model to influence the field forces to point perpendicularly to the edges when the field forces are near the edges, even near weak edges with strong neighbors. In the following, we first introduce how to obtain the geometric information of an edge map.

3.1. Geometric vectors

Strong virtual electric charges in an edge map generally are not independently distributed. Instead, they usually form salient curves called image edge. The field forces near the image edge are expected to point perpendicularly to it. Here, we employ the tangent direction of the image edge as the geometric information to applied in the proposed model. For each virtual electric charge, we use a vector that we call the "geometric vector" to represent the geometric information. Because the gradient of a smoothed gray-value image is approximately orthogonal to the tangent of the im-

age edge, we calculate the geometric vector $\boldsymbol{v} = (v, u)$ for each virtual electric charge at position (x, y) by

$$\begin{aligned} v(x,y) &= -[G_\sigma(x,y) * I(x,y)]_y, \\ u(x,y) &= [G_\sigma(x,y) * I(x,y)]_x, \end{aligned} \tag{6}$$

where $[G_\sigma(x,y) * I(x,y)]_x$ and $[G_\sigma(x,y) * I(x,y)]_y$ are the spatial gradients of the smoothed I along the x-axis and y-axis, respectively. To avoid increasing the noise of the geometric vectors, we do not normalize the geometric vector $\boldsymbol{v}$ for the proposed model. Fig. 1 shows an example of the geometric vectors computed for a 100×100 synthetic ring image that has weak edges with strong neighbors.

3.2. Incorporating geometric vectors into VEF model

Once the geometric vectors for all electric charges have been obtained from Eq. (6), they can be integrated into the VEP model formulated by Eq. (4). We propose a modified model to compute the VEP at location r by

$$P_{\mathrm{AVEF}}(r) = \sum_{k:R_k \neq r}^{N} \frac{e_k}{4\pi\varepsilon_0} \frac{\exp(\lambda|\langle r_k, \boldsymbol{v}\rangle|)}{|r - R_k|}, \tag{7}$$

where r_k denotes $(r - R_k)/|r - R_k|$, which is the direction from electric charge e_k to location r, and $\langle \cdot, \cdot \rangle$ denotes inner product. The new parameter λ is a nonnegative parameter, which plays a very important role because it controls the influence of the geometric vectors on the modified VEP, and further on its corresponding force field. We note the following the properties of the proposed VEP model in Eq. (7) under different values of the parameter λ: (1) When $\lambda = 0$, the value of $\exp(\lambda|\langle r_k, \boldsymbol{v}\rangle|)$ is equal to 1 regardless of the value of $\boldsymbol{v}$. In this case, Eq. (7) becomes Eq. (4). Therefore, the VEP model given in Eq. (4) is a special case of the proposed VEP model with $\lambda = 0$. (2) When λ takes an appropriate positive value, the proposed VEP will have a different intensity distribution from the original VEP. A simple example is given in Fig. 2 to show the differences. As shown in Fig. 2a, the intensity distribution of the original VEP generated by a single electric charge is isotropic, i.e. the intensity of the VEP decreases without directional bias. On the other hand, the intensity distribution of the proposed VEP generated by a single electric charge with geometric vector is anisotropic, as shown in Fig. 2b. That is, the intensity of the potential, as distance increases from the electric charge, will decrease more slowly along the direction of the geometric vector than along the vertical direction of the geometric vector. Therefore, the intensity of the proposed VEP is relatively enhanced along the image edge, even along weak image edges with strong neighbors. It should be pointed out that the directions of vectors $\boldsymbol{v}$ and $-\boldsymbol{v}$ have no difference according to Eq. (7), so we treat them identically. Motivated by this property of the modified VEP, we introduce the terms anisotropic virtual electric potential (AVEP) and, for the corresponding virtual electric field, anisotropic virtual electric field (AVEF).

The AVEF can be obtained by finding the gradient of the AVEP in Eq. (7) as

$$\begin{aligned} F_{\mathrm{AVEF}}(r) &= -\nabla P_{\mathrm{AVEF}}(r) \\ &= \sum_{k:R_k \neq r}^{N} \frac{e_k}{4\pi\varepsilon_0} \frac{\exp(\lambda|\langle r_k, \boldsymbol{v}\rangle|)\left[r_k - \lambda \frac{\langle r_k, \boldsymbol{v}\rangle}{|\langle r_k, \boldsymbol{v}\rangle|}(\boldsymbol{v} - \langle r_k, \boldsymbol{v}\rangle r_k)\right]}{|r - R_k|^2}. \end{aligned} \tag{8}$$

Fig. 2c and d shows examples of the VEF and the AVEF generated by a single electric charge, respectively. It can be seen that the VEF generated by a single electric charge is also isotropic. The VEF forces point to the single electric charge. Their intensities decrease without directional bias from the electric charge to the image border. On the other hand, the AVEF generated by a single electric charge with geometric information is anisotropic. The AVEF forces tend to point to a special line that is parallel to the geometric vector, and the intensity of the AVEF is higher along this special line than in other regions. Due to the anisotropic property of the AVEF, the

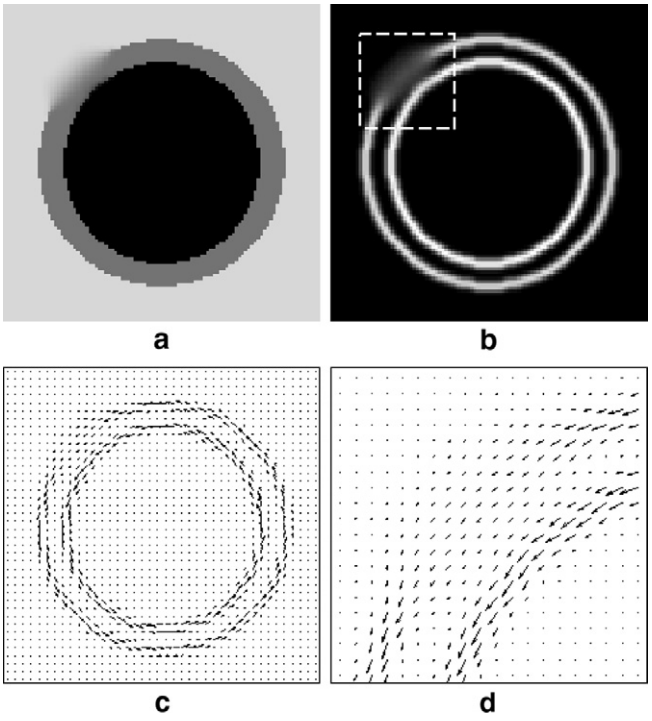

Fig. 1. (a) A synthetic ring image with weak edge. (b) Edge map of the ring image. (c) Geometric vectors of the ring image. (d) Close-up of the geometric vectors inside the dashed box of (b).

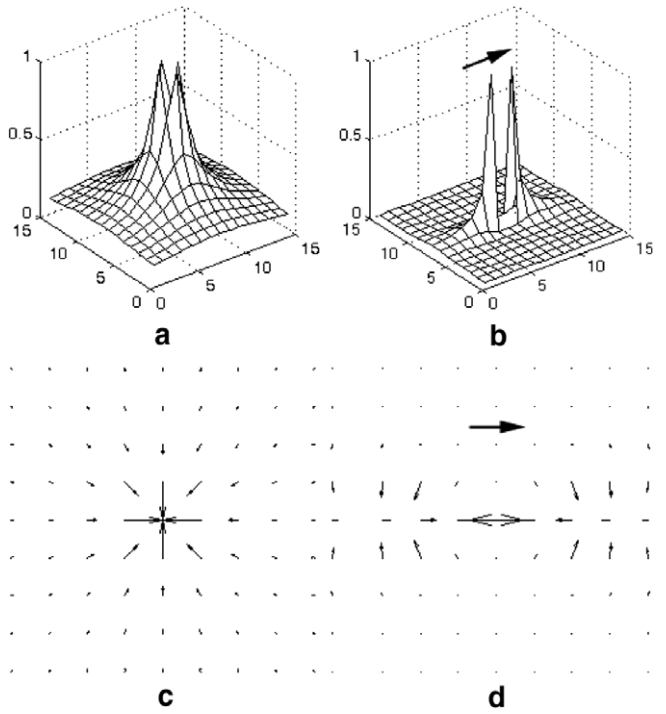

Fig. 2. (a) VEP generated by a single electric charge. (b) AVEP generated by a single electric charge with geometric vector. (c, d) VEF and AVEF fields corresponding to the VEP in (a) and the AVEP in (b). Note that the single electric charge is located at the center of the image domain and the arrow represents the direction of the geometric vector.

field forces will tend to point perpendicularly to image edges when they are near the edges, even near weak edges with strong neighbors, so they have the advantage of preventing active contours from moving across these weak edges. It is seen that the ability of preventing boundary leakage of the proposed model is mainly determined by the parameter λ. When the value of λ increases, the anisotropic property of the proposed AVEF will increase correspondingly. So the proposed AVEF active contour will enhance the ability of avoiding the boundary leakage. However, the AVEF active contour will get to be more sensitive to image noise when λ is too large. On the other hand, when λ becomes smaller, the anisotropic property of the AVEF will decrease correspondingly. The AVEF active contour will have similar performance to the VEF active contour when λ approaches 0.

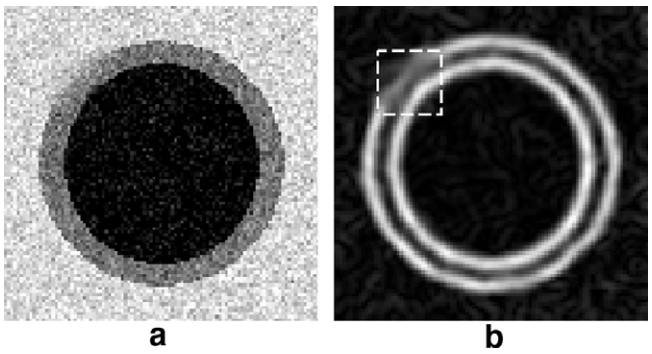

Fig. 4. (a) Noisy ring image. (b) Edge map of the noisy ring image.

4. Experiments

We compared the performance of the AVEF model with that of the VEF as well as the GVF models. We implemented the three different external forces on the Kass active contour framework introduced in Section 2. We used both synthetic and real images in the experiments. In all our experiments, we set $\alpha = 1.0$ and $\beta = 0.0$, and we normalized the edge maps to the range [0,1]. We used $\lambda = 20$ for the proposed AVEF model (except for the following

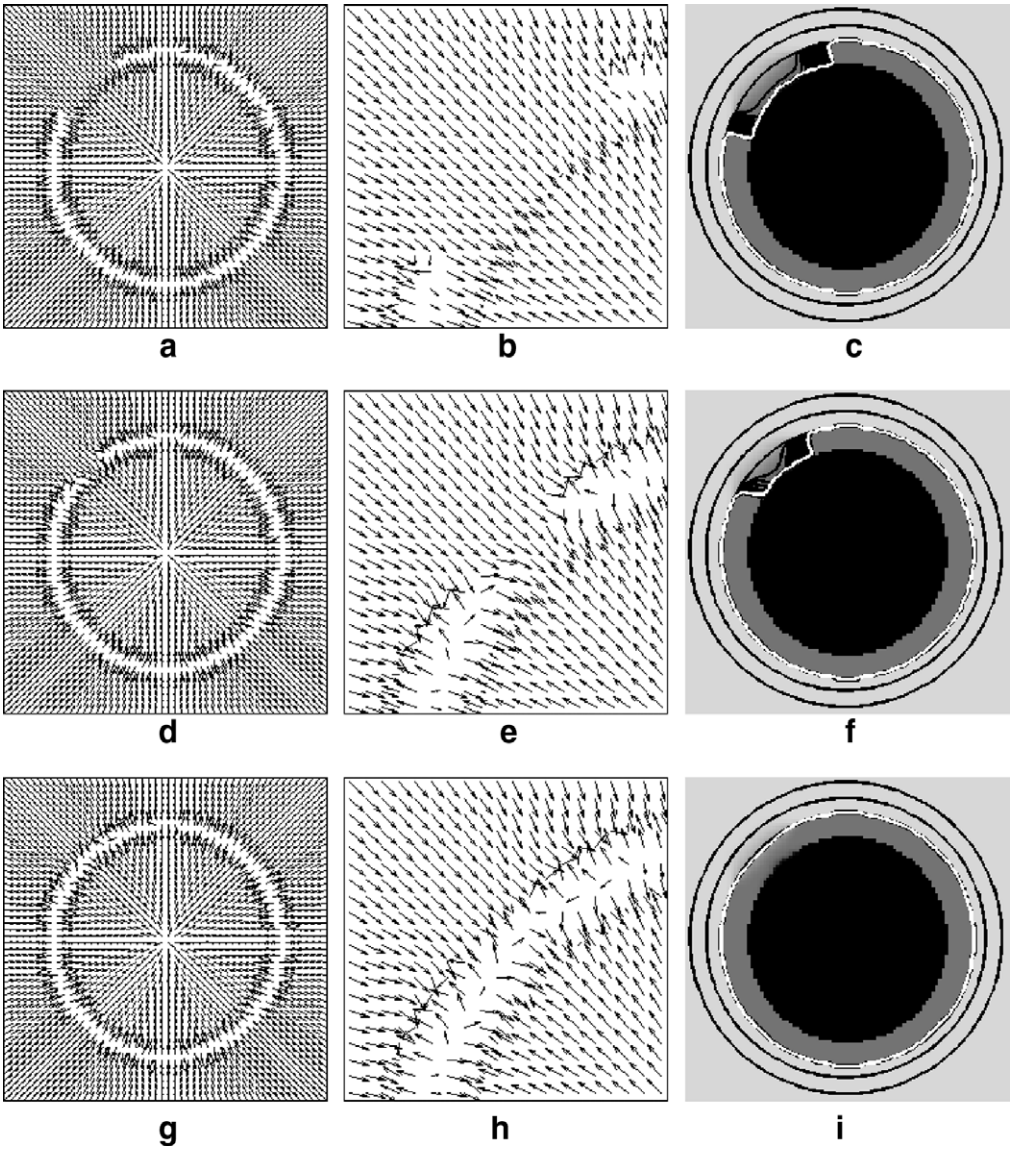

Fig. 3. External force field, close-ups of the force fields at the weak edge and convergence of the active contours. (a)–(c) GVF active contour. (d)–(f) VEF active contour. (g)–(i) AVEF active contour. Note that the white lines represent the active contours at convergence.

experiment that tests the property of the parameter λ), and the same parameter values used in (Xu and Prince's paper, 1998b) for the GVF model.

In the experiments, we used two strategies for saving the computational cost of the AVEF. The first, which was introduced by Park and Chung (2002), was to compute the electric field at location r by summing up the electric fields contributed by the electric charges in a limited circular area around location r, not in the whole image domain. In fact, the implementation of the limited circular area used a squared window which is similar to the disk-shaped structuring element in morphological operations. The second strategy was to remove the electric charges with very low intensities. That is, we regarded an electric charge as noise when it was smaller than a predefined threshold T, and set it to zero in the computation of the force field. Assume that the diameter of

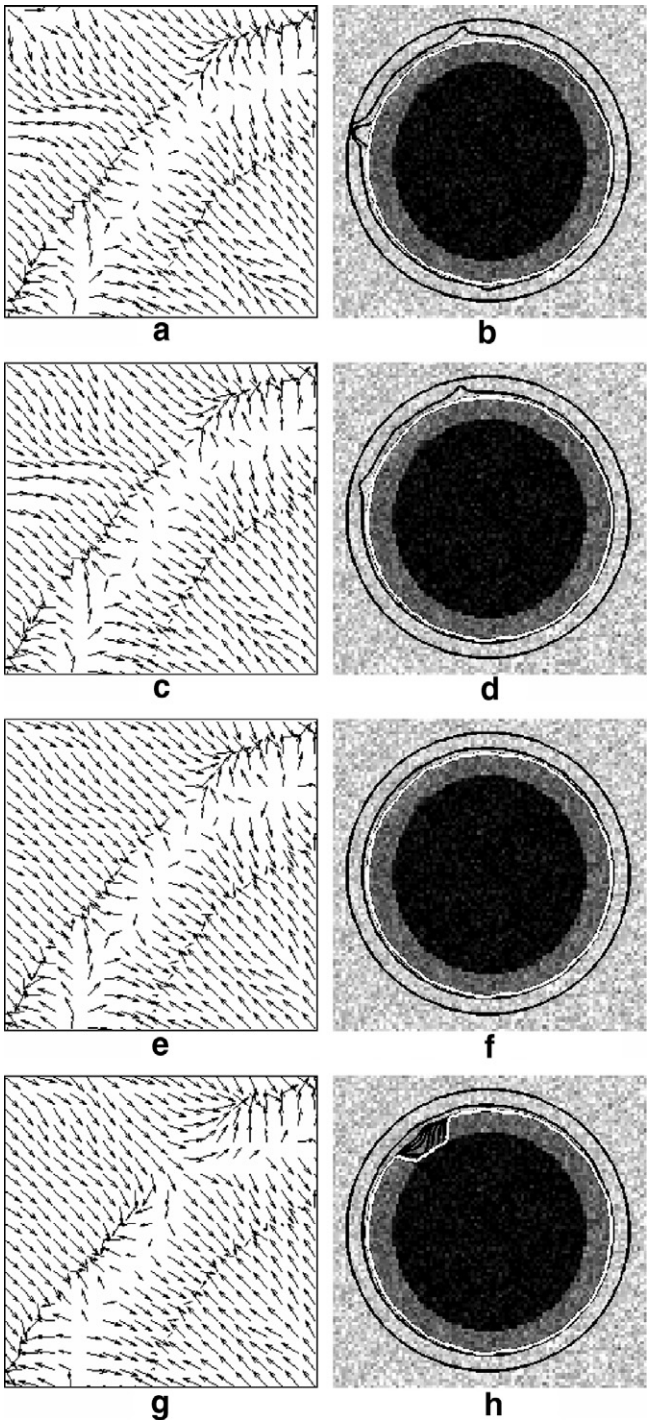

Fig. 5. AEVFs and convergence of the AVEF active contour under different threshold T. (a, c, e and g) AVEFs inside the dashed box of Fig. 4b when the threshold T takes 0, 0.15, 0.3, and 0.45, respectively. (b, d, f and h) the corresponding convergence of the AVEF active contour in segmenting the noisy ring image. Note that the white lines represent the AVEF active contours at convergence.

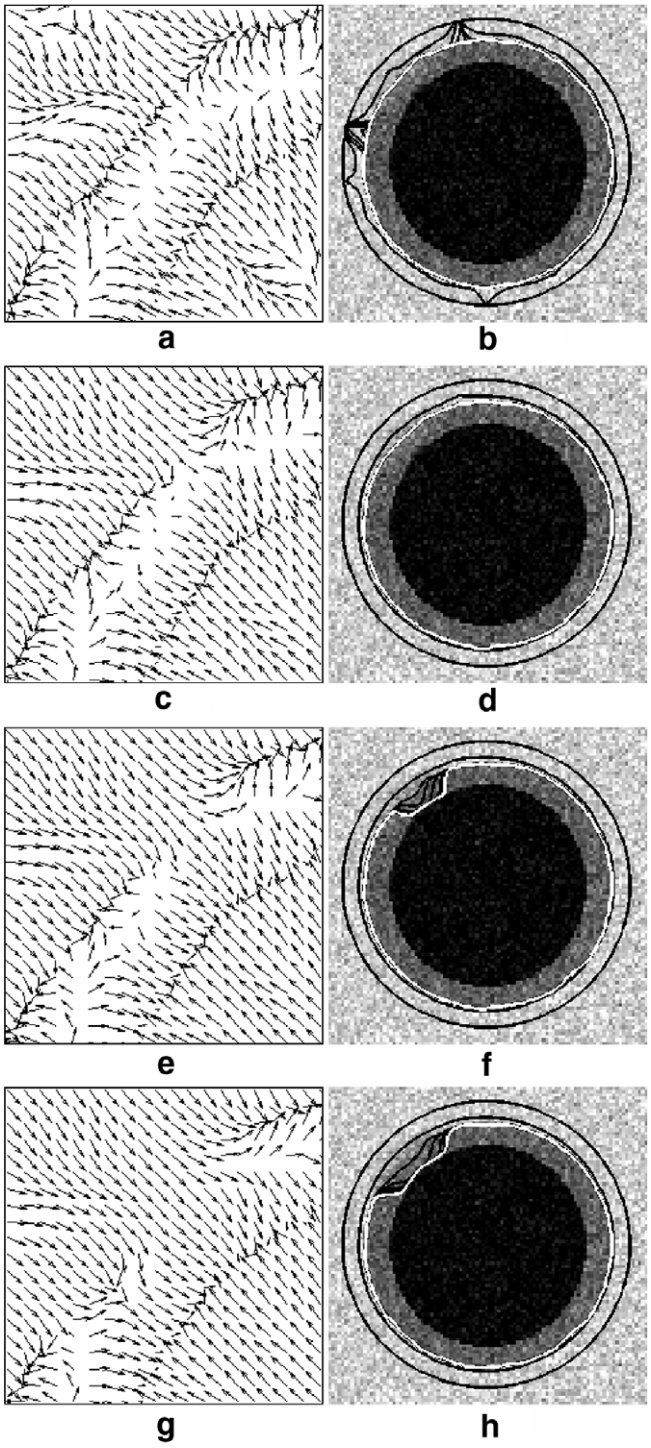

Fig. 6. AEVFs and convergence of the AVEF active contour under different λ. (a, c, e and g) AVEFs inside the dashed box of Fig. 4b when the parameter λ takes 60, 10, 4, and 0, respectively. (b, d, f and h) the corresponding convergence of the AVEF active contour in segmenting the noisy ring image. Note that the white lines represent the AVEF active contours at convergence.

the limited circular area is K, the computational complexity is $O(K^2 \times N)$ for computing the AVEF on an image with N pixels. The experiments show that $K = 100$ is large enough to compute the AVEF for most practical images. According to the experiments, the strategy of setting the threshold T can speed up the computation of the proposed AVEF by a factor of 2.0–3.5 when the threshold T takes the value of 0.15.

We first performed the experiment on a synthetic ring image shown in Fig. 1. Fig. 3 shows the obtained GVF, VEF, AVEF, as well as the convergence of the associated active contours. It is seen from Fig. 3 that all the three force fields have a large capture range. However, the field forces of the GVF and the VEF at the weak edges point toward the strong neighboring edges, and therefore, the GVF and the VEF active contours are driven to move across these week edges to the strong neighboring edges. One the other hand, the AVEF field forces point oppositely along the weak edges, so the AVEF active contour is prevented from moving across these edges and can more accurately conform to the outside boundary of the synthetic ring image.

In order to handle image noise, here we introduce four strategies for the proposed AVEF active contour and conducted associated experiments to validate them. The first strategy is to increase the value of the threshold T, which, however, could result in the increase of the risk of the boundary leakage. The second one is to decrease the value of the parameter λ of the AVEF model. But, reducing λ will lower the anisotropic property of the AVEF correspondingly. This will further lead to weaken the ability of the proposed active contour on handling the boundary leakage. The third one is to increase the value of the parameter σ of the Gaussian filter in computing the edge map f. But, too large of the σ will decrease the accuracy of the boundary extraction, and will also increase the risk of the boundary leakage at week edges. The fourth strategy to increase the value of the parameter α and β, which will also decrease the accuracy of the boundary extraction.

The third and fourth strategies have been considered in the Kass active contour, the GVF active contour and the related works. Here, we just provide two experiments to show how the first and the second strategies perform on noisy images, respectively. Fig. 4 shows the tested ring image and its edge map for the two experiments, where Gaussian noise with a variance of 650 had been added to the ring image. The first experiment shows the influence of the threshold T on segmenting the noisy image by the AVEF active contour. Since the edge map f is normalized into [0,1], the threshold T should also take a value from the range [0,1]. Fig. 5 shows the experimental results when the threshold T takes 0 (i.e. no electric charge is removed), 0.15, 0.3, and 0.45, respectively. It is seen from Fig. 5 that from $T = 0$ to $T = 0.45$ the AVEF gets more smooth and the evolving contour of the AVEF active contour model also gets more smooth, but the boundary leakage happens at $T = 0.45$. This experiment indicates that when the value of the threshold increases, the proposed method will be more robust to image noise in some sense, however, when the threshold becomes too large, the boundary leakages tend to happen in the image segmentations using the AVEF active contour. We found empirically that when the threshold T takes a value from [0,0.3], the proposed active contour works quite well on most natural and medical images. The second experiment shows the influence of the parameter λ on segmenting a noisy image. In this experiment, we set the threshold T to be 0.15. Fig. 6 shows the experimental results of the AVEF active contour when the parameter λ takes 60, 10, 4, and 0, respectively. Note that when the parameter λ is 0, the proposed AVEF is identical to the VEF (Park and Chung, 2002). Combing the cases of $\lambda = 60$, 10, 4, and 0 in Fig. 6 with that of $\lambda = 20$ in Fig. 5c and d, we can see that when the value of the parameter λ decreases, the AVEF will get more smooth, and the evolving contour of the AVEF active contour model also get more smooth, which means that the proposed method becomes more robust to image noise. However, the anisotropic property of the AVEF will also de-

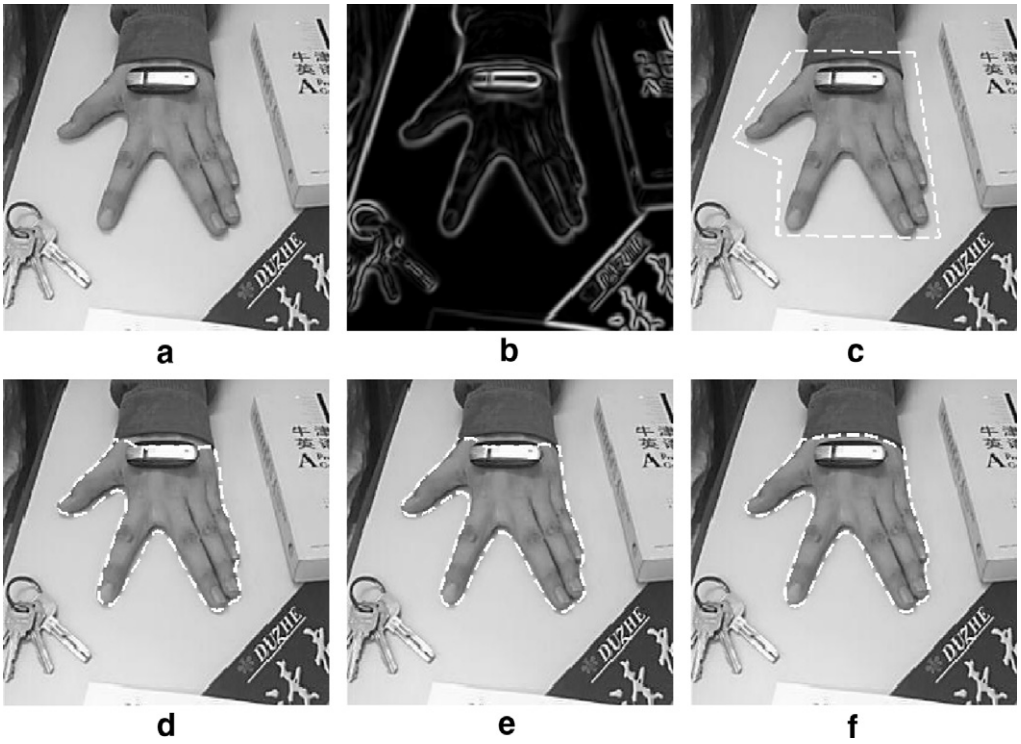

Fig. 7. Segmentation of the hand image. (a) Original hand image. (b) Edge map of the hand image. (c) Initialization of the active contour. (d)–(f) Segmentation results of the GVF, VEF and AVEF active contour, respectively.

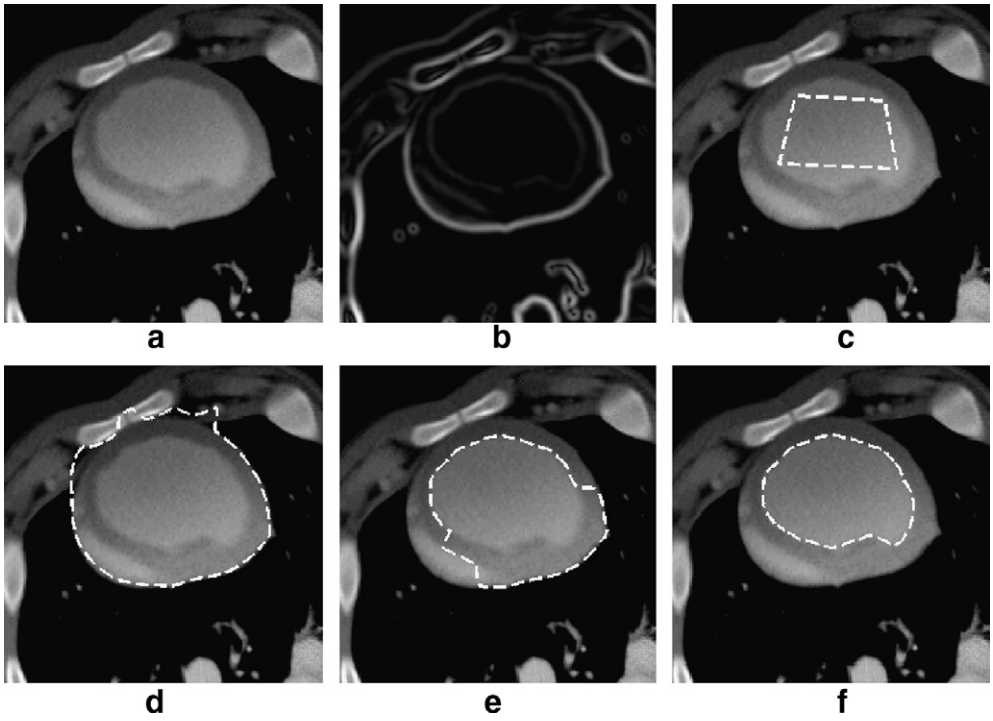

Fig. 8. Segmentation of the cardiac CT image. (a) Original cardiac CT image. (b) Edge map of the cardiac image. (c) Initialization of the active contour. (d)–(f) Segmentation results of the GVF, VEF and AVEF active contour, respectively.

crease, which results in the boundary leakage (as shown in Fig. 6f and g). According to the above experiments, a value between 10 and 40 for λ will generally give satisfactory results for most images, so we chose a middle value from the interval for the parameter λ (i.e. $\lambda = 20$) in the following experiments.

Next, we carried out the experiments on three real images. All of the tested images are 240×240 in size. Fig. 7 shows the segmentation results of a hand image. It is seen that the USB drive on the back of the hand forms a strong edge near the boundary of the hand to be segmented. The initializations are the same for

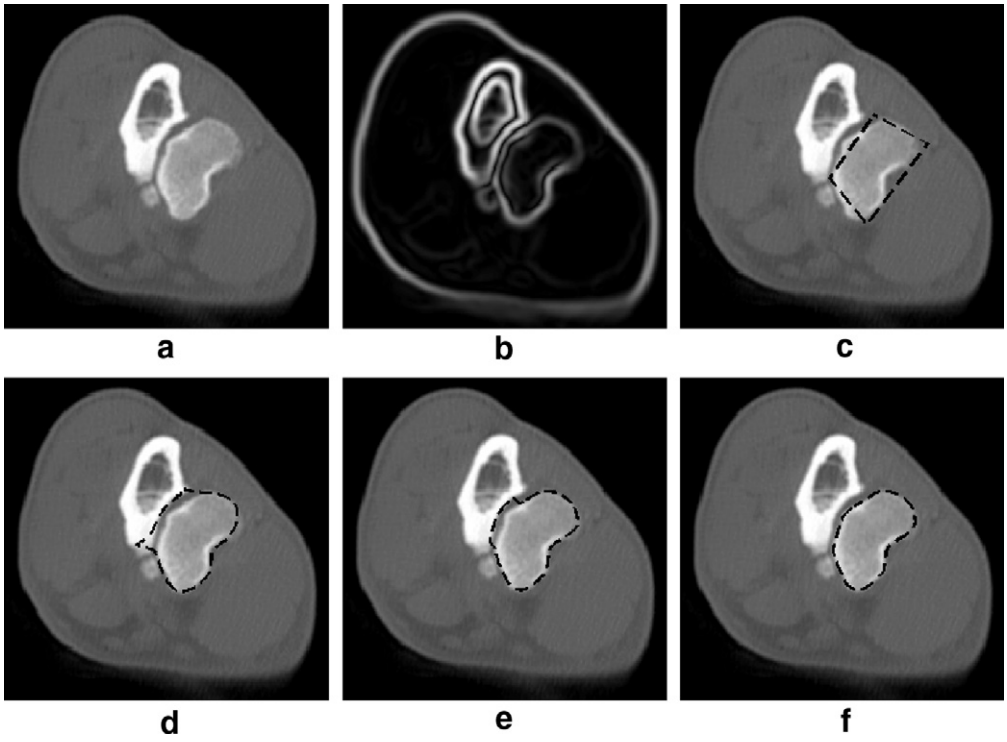

Fig. 9. Segmentation of the elbow CT image. (a) Original elbow CT image. (b) Edge map of the elbow image. (c) Initialization of the active contour. (d)–(f) Segmentation results of the GVF, VEF and AVEF active contour, respectively.

the GVF, VEF, and AVEF active contours. All of these three active contours converge to the concavities formed by the fingers. However, both the GVF and the VEF active contours move across the hand boundary and are attracted to the silent edge formed by the USB drive, only the AVEF active contour converges to the accurate hand boundary. Similarly, Figs. 8 and 9 show the segmentation results of the cardiac and elbow computed tomography (CT) images, respectively. They also demonstrate that the proposed AVEF model has the advantage of preventing contours from moving across weak edges with strong neighbors over the GVF and the VEF models.

5. Conclusion

We have presented a novel external force called anisotropic virtual electric field (AVEF) for active contours. The AVEF is based upon the VEF, which considers each pixel in an edge map as an electric charge in physics. But being different from the VEF, which strictly conform to the electric field in physics, the proposed AVEF employs the geometric information of the edge map to influence the field forces to point perpendicularly to the edges when the field forces are near the edges, even near the weak edges with strong neighbors. Experimental results obtained from both synthetic and real images show that the AVEF is superior to the VEF and the GVF with respect to preventing the active contours from moving across object boundary's weak edges with strong neighbors. The AVEF maintains other desirable properties of the VEF such as large capture range and high processing speed. We note that the anisotropic ability of preventing boundary leakage is mainly determined by the parameter λ in the AVEF. The anisotropic property will enhance with the increase of λ. However, the AVEF active contour will get to be more sensitive to image noise when λ is too large. We also studied several strategies to increase the robustness of the proposed AVEF active contour against image noise. In particular, the influence of the threshold T and the parameter λ on segmenting noisy images were investigated experimentally. Increasing the threshold T or decreasing the parameter λ can lead to better segmentation performance when the image contains noise. However, a very big T or small λ might weaken the ability of the proposed model on handling the boundary leakage problem. According to our experiments, a value between 0 and 0.3 for T and a value between 10 and 40 for λ and will generally give satisfactory results for most images.

Acknowledgements

The authors would like to thank the anonymous reviewers for their valuable comments and suggestions, especially thank the reviewer who also kindly helps us edit the exposition of this paper. This work was supported in part by a Grant (#68506-00-37) from The City University of New York PSC-CUNY Research Award Program. This work was also supported in part by the NSFC (No. 60633030), the NSF of Guangdong (No. 04205407 and No. 06023191), and the 973 Program (No. 2006CB303104).

References

Caselles, V., Catte, F., Coll, T., Dibos, F., 1993. A geometric model for active contours. Numer. Math. 66, 1–31.
Caselles, V., Kimmel, R., Sapiro, G., 1997. Geodesic active contours. Internat. J. Comput. Vision 22 (1), 61–79.
Chan, T.F., Vese, L.A., 2001. Active contours without edges. IEEE Trans. Image Process. 10 (2), 266–277.
Chang, H.H., Valentino, D.J., 2006. Image segmentation using a charged fluid method. J. Electron. Imaging 15 (2). Art. No. 023011.
Cheng, J., Foo, S.W., 2006. Dynamic directional gradient vector flow for snakes. IEEE Trans. Image Process. 15 (6), 1563–1571.
Chuang, C.H., Lie, W.N., 2004. A downstream algorithm based on extended gradient vector flow field for object segmentation. IEEE Trans. Image Process. 13 (10), 1379–1392.
Cremers, D., Soatto, S., 2005. Motion competition: A variational approach to piecewise parametric motion segmentation. Internat. J. Comput. Vision 62 (3), 249–265.
Honea, D.M., Snyder, W.E., Bilbro, G.L., 2002. Active contours using a potential field. In: Proc. 16th Internat. Conf. on Pattern Recognition (ICPR'02), vol. 2, pp. 757–760.
Jacob, M., Blu, T., Unser, M., 2004. Efficient energies and algorithms for parametric snakes. IEEE Trans. Image Process. 13 (9), 1231–1244.
Jalba, A.C., Wilkinson, M.H., Roerdink, J.B., 2004. CPM: A deformable model for shape recovery and segmentation based on charged particles. IEEE Trans. Pattern Anal. Machine Intell. 26 (10), 1320–1335.
Kass, M., Witkin, A., Terzopoulos, D., 1988. Snakes: Active contour models. Internat. J. Comput. Vision 1 (4), 321–331.
Li, C., Liu, J., Fox, M.D., 2005. Segmentation of external force field for automatic initialization and splitting of snakes. Pattern Recognition 38 (11), 1947–1960.
Malladi, R., Sethian, J., Vemuri, B., 1995. Shape modeling with front propagation: A level set approach. IEEE Trans. Pattern Anal. Machine Intell. 17 (2), 158–175.
Mansouri, A.R., 2002. Region tracking via level set PDEs without motion computation. IEEE Trans. Pattern Anal. Machine Intell. 24 (7), 947–961.
Mansouri, A.R., Sirivong, B., Konrad, J., 2003. Multiple motion segmentation with level sets. IEEE Trans. Image Process. 12 (2), 201–220.
Paragios, N., Deriche, R., 2000. Geodesic active contours and level sets for the detection and tracking of moving objects. IEEE Trans. Pattern Anal. Machine Intell. 22 (3), 266–280.
Paragios, N., Deriche, R., 2002. Geodesic active regions: A new framework to deal with frame partition problems in computer vision. J. Visual Comm. Image Represent. 13 (1–2), 249–268.
Paragios, N., Mellina-Gottardo, O., Ramesh, V., 2004. Gradient vector flow fast geometric active contours. IEEE Trans. Pattern Anal. Machine Intell. 26 (3), 402–407.
Park, H.K., Chung, M.J., 2002. External force of snake: Virtual electric field. Electron. Lett. 38 (24), 1500–1502.
Park, H., Schoepflin, T., Kim, Y., 2001. Active contour model with gradient directional information: Directional snake. IEEE Trans. Circ. Systems Video Technol. 11 (2), 252–256.
Ray, N., Acton, S.T., 2004. Motion gradient vector flow: An external force for tracking rolling leukocytes with shape and size constrained active contours. IEEE Trans. Med. Imaging 23 (12), 1466–1478.
Tang, J., Millington, S., Acton, S.T., Crandall, J., Hurwitz, S., 2006. Surface extraction and thickness measurement of the articular cartilage from MR images using directional gradient vector flow snakes. IEEE Trans. Biomed. Eng. 53 (5), 896–907.
Xie, X., Mirmehdi, M., 2004. RAGS: Region-aided geometric snake. IEEE Trans. Image Process. 13 (5), 640–652.
Xu, C., Prince, J.L., 1998a. Generalized gradient vector flow external forces for active contours. Signal Process. 71 (2), 131–139.
Xu, C., Prince, J.L., 1998b. Snakes, shapes, and gradient vector flow. IEEE Trans. Image Process. 7 (3), 359–369.
Yuan D., Lu, S., 2002. Simulated static electric field (SSEF) snake for deformable models. In: Proc. 16th Internat. Conf. on Pattern Recognition (ICPR'02), vol. 1, pp. 83–86.
Zhu, G., Zeng, Q., Wang, C., 2006a. Dual geometric active contour for image segmentation. Opt. Eng. 45 (8). Art. No. 080505.
Zhu, G., Zeng, Q., Wang, C., 2006b. Simultaneously improving the global and local properties of virtual electric field. Electron. Lett. 42 (17), 967–968.